ACS Catalysis

Perspective

Cite This: ACS Catal. 2018, 8, 8121−8129

pubs.acs.org/acscatalysis

Understanding Surface-Mediated Electrochemical Reactions: CO_2 Reduction and Beyond

Marco Dunwell,[†] Wesley Luc,[†] Yushan Yan,*[D] Feng Jiao,*[D] and Bingjun Xu*[D]

Center for Catalytic Science and Technology, Department of Chemical and Biomolecular Engineering, University of Delaware, Newark, Delaware 19716, United States

ABSTRACT: Understanding reaction pathways and mechanisms for electrocatalytic transformation of small molecules (e.g., H_2O, CO_2, and N_2) to value-added chemicals is critical to enabling the rational design of high-performing catalytic systems. Tafel analysis is widely used to gain mechanistic insights, and in some cases, has been used to determine the reaction mechanism. In this Perspective, we discuss the mechanistic insights that can be gained from Tafel analysis and its limitations using the simplest two-electron CO_2 reduction reaction to CO on Au and Ag surfaces as an example. By comparing and analyzing existing as well as additional kinetic data, we show that the Tafel slopes obtained on Au and Ag surfaces in the kinetically controlled region (low overpotential) are consistently ~59 mV dec^{-1}, regardless of whether catalysts are polycrystalline or nanostructured in nature, suggesting that the initial electron transfer ($CO_2 + e^- \rightarrow CO_2^-$) is unlikely to be the rate-limiting step. In addition, we demonstrate how initial mechanistic assumptions can dictate experimental design, the result of which could in turn bias mechanistic interpretations. Therefore, as informative as Tafel analysis is, independent experimental and computational techniques are necessary to support a proposed mechanism of multielectron electrocatalytic reactions, such as CO_2 reduction.

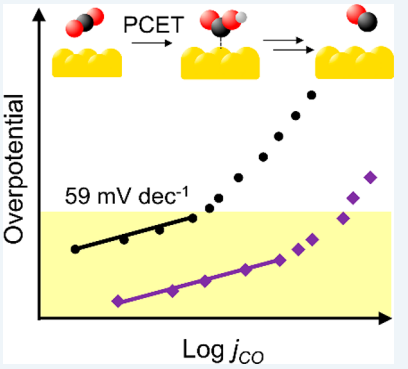

KEYWORDS: *Tafel slope, carbon dioxide, electroreduction, electrokinetics, overpotential*

INTRODUCTION

The surface-mediated electrochemical conversion of small molecules such as H_2O, CO_2, and N_2 to value-added chemicals using renewable energy is a promising strategy for growing sustainable chemical production and energy storage infrastructure.[1−3] Upgrading these small molecules typically involves multiple electron and proton transfers and can produce many products each with a number of possible reaction intermediates. This complexity presents challenges in the elucidation of molecular-level reaction mechanisms, which are critical to the design of efficient, selective, and stable electrocatalysts.[4]

A variety of experimental techniques have been used to investigate the reaction pathways and mechanisms of surface-mediated electrochemical reactions, from feeding suspected intermediate species as reactants[5−7] to utilizing spectroscopic techniques to probe reaction intermediates,[8,9] each with their own advantages and disadvantages. One of the most common methods in electrocatalysis is Tafel analysis, in which the quantitative dependence of the partial current density toward a specific product (the electrochemical reaction rate) on the applied potential (Tafel slope) is determined.[10] The experimentally observed Tafel slopes can then be compared to theoretically derived slopes by assuming different rate-limiting steps (RLS) and quasi-equilibrated steps in a proposed reaction mechanism. By comparing the experimentally measured Tafel slope with those derived on the basis of a proposed mechanism and RLS, researchers are able to either reject or support proposed mechanistic pathways. However, Tafel analysis does have significant limitations. For example, it cannot differentiate two mechanisms that share the same expected Tafel slope, which is frequently the case for complex reactions involving multiple electron and proton transfers. Furthermore, initial mechanistic assumptions can influence experimental design, which could in turn bias mechanistic interpretations.

In this Perspective, we use the simplest two-electron CO_2 reduction reaction (CO_2RR), the catalytic conversion of CO_2 to CO on Au and Ag surfaces, as an example to demonstrate the complexity and challenges associated with commonly used electrochemical techniques for elucidating the reaction pathways and mechanisms. Through a detailed comparison and analysis of both existing and new electrokinetic data, we show that the results of these mechanistic studies strongly depend on experimental design, which is dictated by the assumed reaction mechanism. The Perspective will discuss the mechanistic insights gained from Tafel analysis, as well as considerations in choosing experimental parameters when conducting Tafel analysis to ensure measured rates are dictated by electrokinetics rather than being convoluted by mass transport limitations. Particular emphasis is placed on how these variations in Tafel analysis within the existing literature result

Received: June 5, 2018
Revised: July 19, 2018
Published: July 20, 2018

DOI: 10.1021/acscatal.8b02181
ACS Catal. 2018, 8, 8121−8129

in different conclusions about the possible reaction pathways and the RLS. Further, the Perspective will demonstrate how the assumed reaction mechanism and the RLS can dictate experimental design, including which variables must be controlled to obtain meaningful kinetic data. For example, in the case of CO_2RR to CO, the choice of reference scale between the standard hydrogen electrode (SHE) and reversible hydrogen electrode (RHE), which should be equivalent in principle, can each produce seemingly conclusive results that reinforce differing initial mechanistic assumptions. As such, we hope to convey the challenges associated with these experimental methods and emphasize the necessity of developing advanced *operando* spectroscopic techniques and computational methods to help further elucidate the reaction pathways and mechanisms for the CO_2RR specifically, as well as for the electrochemical upgrading of other small molecules.

MECHANISTIC INSIGHTS THROUGH TAFEL ANALYSIS

Derivations and Limitations of Tafel Analysis. Although Tafel analysis has been used to propose and verify reaction mechanisms (e.g., hydrogen evolution reaction (HER),[10−12] hydrogen oxidation reaction (HOR),[10,13,14] oxygen reduction reaction,[10,15−18] oxygen evolution reaction,[10,19,20] and ethanol oxidation reaction),[21] it is imperative to note that Tafel analysis has limitations. Most notably, Tafel analysis is only appropriate within a specific overpotential range. For an electrochemical reaction of the form given in eq 1, the full Butler−Volmer equation (eq 2) can be simplified to the Tafel equation (eq 3) only if the overpotential is sufficiently high so that the rate of the reverse reaction is negligible comparing to that of the forward reaction, that is, $\exp\left(\frac{\eta\beta F}{RT}\right) \ll \exp\left(\frac{\eta(\beta-1)F}{RT}\right)$.[22]

$$O + ne^- \leftrightarrow R \tag{1}$$

$$j = nFk^0\left[a_R \exp\left(\frac{\eta\beta F}{RT}\right) - a_O \exp\left(\frac{\eta(\beta-1)F}{RT}\right)\right] \tag{2}$$

$$j = -nFk^0\left[a_o \exp\left(\frac{\eta(\beta-1)F}{RT}\right)\right] \tag{3}$$

In eqs 2 and 3, $\eta = E - E_{equilibrium}$, and β is the symmetry factor. To clarify, η is negative for reduction reactions such as CO_2RR, and the term overpotential in this Perspective refers to the magnitude of η, i.e., $|\eta|$. Thus, a higher overpotential corresponds to a lower (or more negative) electrode potential. The overpotential must be kept sufficiently low so that the reaction rate is kinetically controlled in determining Tafel slopes. Otherwise the observed Tafel slope will be convoluted by mass transport limitations. For example, owing to very fast kinetics, Tafel analysis of the HOR/HER on Pt using the rotating disk electrode method were plagued by transport limitations which caused an apparent Tafel slope of ∼30 mV dec^{-1}, suggesting a rate-limiting Tafel step (i.e., $H_2 \leftrightarrow 2H_{ad}$).[14] However, more recent work using a H_2 pump configuration to improve mass transport has shown a Tafel slope of ∼118 mV dec^{-1}, consistent with either a Volmer ($H_{ad} \leftrightarrow H^+ + e^-$) or Heyrovsky ($H_2 \leftrightarrow H_{ad} + H^+ + e^-$) RLS.[14,23] Moreover, Tafel slopes, even when measured properly, in many cases do not correspond to a unique mechanism as several proposed mechanisms could lead to the same expected Tafel slope. This is due to two primary reasons: (1) measured Tafel slopes are only impacted on the RLS and steps before RLS, and (2) mechanisms with different RLS and/or the steps before RLS could result in the same expected Tafel slope. This case is also illustrated in the mechanistic investigation of the HOR/HER, where a Tafel slope of 118 mV dec^{-1} indicates that either the Volmer or Heyrovsky step is limiting, but does not distinguish between the two. Thus, as informative as Tafel analysis is, additional characterization is often needed to unequivocally prove a proposed mechanism.

Experimentally Determined Tafel Slopes for the CO_2RR on Au and Ag Surfaces. For the simplest two-electron CO_2RR to CO on Au, different Tafel slope values (56−140 mV dec^{-1}) have been reported,[24−30] leading to many different mechanistic proposals. Figure 1 summarizes previous Tafel analyses and illustrates how the experimentally derived Tafel slope is highly dependent on the region of applied potentials employed. While most of literature reported a Tafel slope near 118 mV dec^{-1}, studies of CO_2RR to CO at low overpotentials (less negative than −0.4 V vs RHE) have consistently exhibited slopes near 59 mV dec^{-1} (Figure 1, black solid circles and open purple traces). Kanan et al. have previously ascribed the lower Tafel slope observed on oxide-derived Au electrodes to a change in the RLS due to stabilization of the proposed $*CO_2^-$ intermediate.[24] Meanwhile, our previous work showed that even bulk, polycrystalline Au electrodes also exhibited a Tafel slope near 59 mV dec^{-1} at sufficiently low overpotentials.[25] We therefore propose that the previously observed Tafel slopes near 118 mV dec^{-1} are a result of those experiments being conducted at high overpotentials, at which measured CO production rates are not strictly determined by electrokinetics. Indeed, for each of the polycrystalline Au experiments conducted at higher overpotentials (Figure 1, solid red, purple, and gold symbols), the Tafel slope exhibits a noticeable residual curvature when approaching lower overpotentials (less-negative potentials), indicating that measured rates in these experiments are likely impacted by nonkinetic factors, such as mass transport limitations.[24,29,31] For example, although Kanan et al. reported

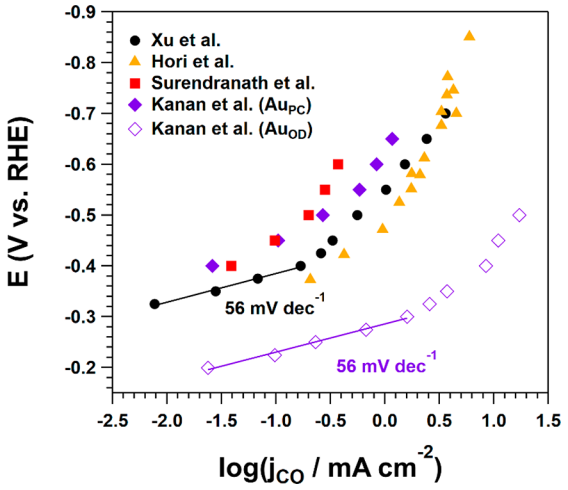

Figure 1. Representative Tafel plots for polycrystalline Au from Xu et al. (black circles, ref 25), Hori et al. (gold triangles, ref 26), Surendranath et al. (red squares, ref 29), and Kanan et al. (solid purple diamonds, ref 24) and oxide derived Au (open purple diamonds, ref 24). Solid lines represent linear fits between points with slopes of the indicated value.

DOI: 10.1021/acscatal.8b02181
ACS Catal. 2018, 8, 8121−8129

a slope of 114 mV dec^{-1} for polycrystalline Au, the slope using data points at the lowest measured overpotentials (−0.4 and −0.45 V vs RHE), decreases to 83 mV dec^{-1}.[24] A similar trend holds in a recent report by Surendranath et al. where Tafel slopes of 125, 140, and 167 mV dec^{-1} can be calculated using the two, three, and four lowest overpotential points, respectively.[29] Moreover, in our previous work with Au foil electrodes, Tafel slopes of 134 and 167 mV dec^{-1} were observed using data from −0.4 to −0.425 V and −0.4 to −0.45 V (vs RHE), respectively.[25]

There is a strong parallel in measured Tafel slopes on Au and Ag surfaces, both exhibiting high CO selectivity.[31] Despite the majority of existing work suggesting a Tafel slope of ∼118 mV dec^{-1} on bulk Ag, Tafel slope values close to 59 mV dec^{-1} (64 and 58 mV dec^{-1}) were measured on nanoparticle and nanoporous Ag electrodes at low overpotentials (less negative than −0.5 V vs RHE, Figure 2).[32,33] Like Kanan et al., Jiao et al. initially attributed the shift in Tafel slope to a change in the RLS of the reaction, owing to an increase in step-site density for the nanostructured electrodes.[33] However, measurements on bulk polycrystalline Ag foils at low overpotentials (less negative than −0.5 V vs RHE) in this work show a similar slope (67 mV dec^{-1}) to that of nanostructured Ag. Like Au, Ag most likely has a transport-free Tafel slope of ∼59 mV dec^{-1}, and previous measurements showing slopes near 118 mV dec^{-1} are due to transport limitations caused by the range of current density and potential employed. Therefore, it is critical to ensure Tafel slopes are measured under conditions controlled only by electrokinetics. In addition to current density, electrode potential could also play a decisive role in determining whether the measured rate is dictated by electrokinetics, as will be discussed in detail in the following section.

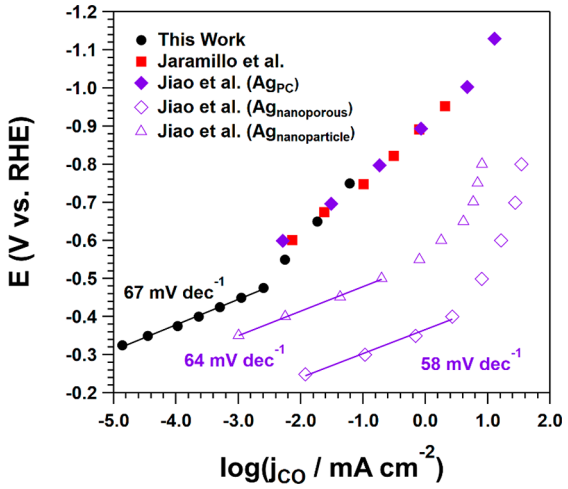

Figure 2. Representative Tafel plots for polycrystalline Ag from this work (black circles), Jaramillo et al. (red squares, ref 32), and Jiao et al. (solid purple diamonds, ref 33). Open purple diamonds and triangles represent Tafel data on nanoporous and nanoparticles, respectively (ref 33). Solid lines represent linear fits between points with slopes of the indicated value.

Impact of Electrode Potential on Measured Rates. Mass transport limitations in electrode-surface-mediated reactions are caused by the slow rate of transport of reactants to, or products from, the electrode relative to the rate of the electrode reaction (current density).[14,22] In addition, the reorganization of ions in the electrical double layer in response to the electrode potential could also have an impact on the mass transport. Cationic species tend to crowd the outer Helmholtz plane (OHP) of the electrical double layer at lower electrode potential due to electrostatic attraction.[22,34] These electrostatically bound cations have been shown to interact or even displace adsorbed species.[25,35] It is likely that these cations could to a certain extent limit the access of reactant to the surface and cause a mass transport limitation. This effect will be more pronounced at lower electrode potentials, as the OHP will be increasingly crowded by cations drawn by negatively charged electrode surface and the electrostatic interaction between the cations and the surface will be stronger. This phenomenon was illustrated using attenuated total reflectance surface enhanced infrared spectroscopy (ATR-SEIRAS) with CO as a probe molecule. The potential was cycled between 1.0 and −0.8 V vs SHE in CO-saturated 0.1 M $KClO_4$ electrolyte on an Au film electrode (Figure 3). At high potentials (>0.8 V), the adsorbed CO band (∼2100 cm^{-1}) disappears due to CO oxidation to CO_2.[36−39] Interestingly, the adsorbed CO coverage also decreases below 0.2 V vs SHE and desorbs completely below −0.4 V vs SHE. As detailed in our previous work, the desorption of CO below 0.4 V vs SHE is due to displacement of the weakly bound CO by K^+ in the OHP drawn to the negatively charged electrode.[25,35] In the case of CO_2 reduction, as the electrode potential is decreased, the electrostatic attraction between electrolyte cations and the electrode increases, forming a potentially site-blocking layer of cations in the OHP in addition to displacing produced CO. Although the observed Tafel slopes on polycrystalline Au (∼118 mV dec^{-1}) and oxide-derived Au (∼56 mV dec^{-1}) were measured in the same current density region, mass transport limitations have a more pronounced impact on the measured Tafel slope on polycrystalline Au due to the lower electrode potential needed to achieve the same current density (∼0.15 V lower as compared to that on oxide-derived Au) due to its lower activity. The dependence of the composition of the electrochemical interface on electrode potential (accumulation of cationic and anionic species at low and high potentials, respectively) makes the electrode potential a defining parameter, along with the current density, for determining the kinetically controlled potential region and therefore a key parameter in the design of electrokinetic experiments. As a result, Tafel slopes measured at low current densities and electrode potentials without significant electrolyte/electrode interactions are more reliable (i.e., the Tafel slope for the CO_2RR on Ag and Au is 59 mV dec^{-1}). Although it is frequently not practical to conduct electrokinetic investigations at or close to the potential of zero charge (PZC), where the interaction between ions in the electrolyte and the electrode surface is minimal, as in the case of CO_2RR, the closer the potential range investigated is to PZC, the less likely that the measured kinetic parameters are impacted by the ion/electrode interaction.

Expected Tafel Slopes Based on Common CO_2RR Mechanisms. As previously alluded to, measured Tafel slopes could provide valuable, but often not definitive, insights into reaction mechanisms. To facilitate the discussion, we summarize three proposed reaction pathways that are most commonly invoked in the literature (Table 1) and the expected Tafel slope assuming each step as the RLS and low surface coverage of any adsorbed intermediate (i.e., coverage of unoccupied surface sites (θ^*) approaches unity). The

DOI: 10.1021/acscatal.8b02181
ACS Catal. 2018, 8, 8121−8129

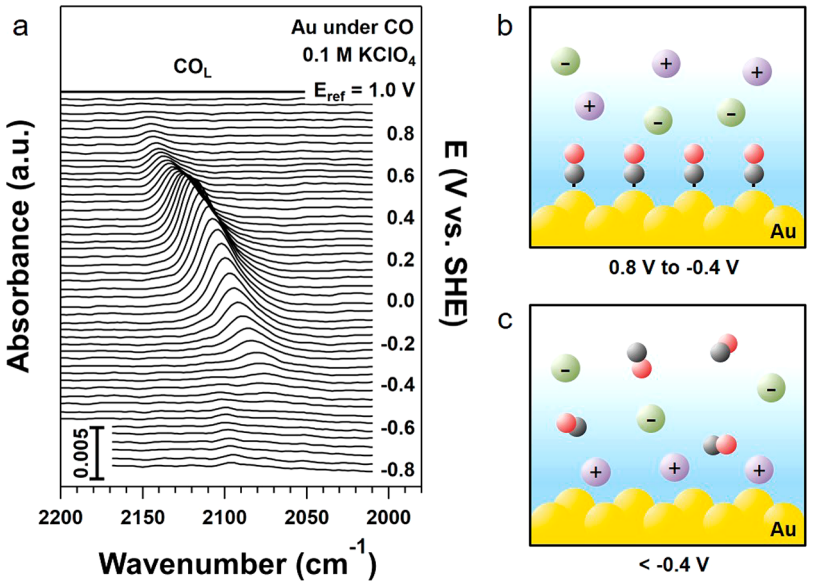

Figure 3. (a) ATR-SEIRA spectra (4 cm^{-1} resolution, 8 co-added scans) a linear potential sweep at 5 mV s^{-1} from −0.8 to 1.0 V vs SHE on chemically deposited Au film electrode in 0.1 M $KClO_4$ under continuous CO purge. Reference spectrum collected at 1.0 V. (b) Schematic representation of CO and electrolyte ions in the double layer between 0.8 and −0.4 V vs SHE and (c) below −0.4 V vs SHE.

Table 1. Proposed Rate Expressions and Corresponding Tafel Slopes

	step	rate expression[b,d]	type[a]	Tafel slope	$[H^+]$ order[c]
A.1	$CO_2 + e^- + * \leftrightarrow (CO_2^-)_{ad}$	$j_{CO} = Fk^0 a_{CO_2}\theta_* \exp\left(\frac{E(\beta-1)F}{RT}\right)$	ET	118	0
A.2	$(CO_2^-)_{ads} + H_2O \leftrightarrow COOH_{ad} + OH^-$	$j_{CO} = Fk^0 K_{A.1} a_{CO_2} \exp\left(-\frac{EF}{RT}\right)$	PT	59	0
A.3	$COOH_{ads} + H_2O + e^- \leftrightarrow CO_{ad} + OH^-$	$j_{CO} = Fk^0 \frac{K_{A.1}K_{A.2}a_{CO_2}a_{H^+}}{K_W} \exp\left(\frac{EF}{RT}(\beta-2)\right)$	PCET	39	1
A.4	$CO_{ad} \leftrightarrow CO + *$	$j_{CO} = Fk^0 \frac{K_{A.1}K_{A.2}K_{A.3}a_{CO_2}a_{H^+}^2}{K_W^2} \exp\left(-\frac{2EF}{RT}\right)$	D	30	2
B.1	$CO_2 + H_2O + e^- + * \leftrightarrow COOH_{ad} + OH^-$	$j_{CO} = Fk^0 a_{CO_2}\theta_* \exp\left(\frac{E(\beta-1)F}{RT}\right)$	PCET	118	0
B.2	$COOH_{ad} + H_2O \leftrightarrow COOH_{ad}\cdots H^+ + OH^-$	$j_{CO} = Fk^0 \frac{K_{B.1}a_{CO_2}a_{H^+}}{K_W} \exp\left(-\frac{EF}{RT}\right)$	PT	59	1
B.3	$COOH_{ad}\cdots H^+ + e^- \leftrightarrow CO_{ad} + H_2O$	$j_{CO} = Fk^0 \frac{K_{B.1}K_{B.2}a_{CO_2}a_{H^+}^2}{K_W^2} \exp\left(\frac{EF}{RT}(\beta-2)\right)$	ET	39	2
B.4	$CO_{ad} \leftrightarrow CO + *$	$j_{CO} = Fk^0 \frac{K_{B.1}K_{B.2}K_{B.3}a_{CO_2}a_{H^+}^2}{K_W^2} \exp\left(-\frac{2EF}{RT}\right)$	D	30	2
C.1	$CO_2 + H_2O + e^- + * \leftrightarrow COOH_{ad} + OH^-$	$j_{CO} = Fk^0 a_{CO_2}\theta_* \exp\left(\frac{E(\beta-1)F}{RT}\right)$	PCET	118	0
C.2	$COOH_{ad} + H_2O + e^- \leftrightarrow CO_{ad} + H_2O + OH^-$	$j_{CO} = Fk^0 \frac{K_{C.1}a_{CO_2}a_{H^+}}{K_W} \exp\left(\frac{EF}{RT}(\beta-2)\right)$	PCET	39	1
C.3	$CO_{ad} \leftrightarrow CO + *$	$j_{CO} = Fk^0 \frac{K_{C.1}K_{C.2}a_{CO_2}a_{H^+}^2}{K_W^2} \exp\left(-\frac{2EF}{RT}\right)$	D	30	2

[a]Assuming a β value of 0.5. [b]Reduction currents are negative based on the convention in eq 2; for clarity, negative signs have been removed for current density in Table 1. [c]ET: electron transfer, PT: proton transfer, PCET: proton-coupled electron transfer, D: desorption [d]Assuming water, rather than bicarbonate or hydronium ions, as the proton donor.

assumption of low surface coverage of adsorbed intermediates is justified by our recent spectroscopic investigation demonstrating that no vibrational band corresponding to adsorbed intermediate, including $CO_{(ad)}$, is present at typical electrode potentials applied in the CO_2RR.[25] Additionally, adsorbed hydrogen coverage is assumed to be negligible as no band related to atop-bound hydrogen is observed spectroscopically, and computational work shows that the hydrogen binding energy is significantly weaker than CO binding energy on Au, so that CO coverage should be higher than that of

DOI: 10.1021/acscatal.8b02181
ACS Catal. 2018, 8, 8121−8129

hydrogen.[25,40] Finally, although electrostatically bound cations may act to prevent transport to the surface, effectively decreasing θ_*, as suggested at high overpotentials, our mechanistic hypothesis is based on the behavior at the low overpotentials (<0.4 V) only, so that cations effects should be minimized. As a result, we assume that cations have a negligible impact on available active sites for the purpose of kinetic derivations. The most commonly proposed mechanism (pathway A) involves an initial electron transfer (ET) to CO_2 to form an adsorbed, negatively charged CO_2 intermediate ($*CO_2^-$), which is then reduced to CO via a proton transfer (PT) step followed by a final proton-coupled electron transfer (PCET) before desorption, as in steps A.1−A.3 (referred to as the ET pathway, or pathway A in Table 1).[24,26−29] Alternatively, it has been proposed that the reaction proceeded through an initial PCET to form an adsorbed carboxyl species (*COOH), followed by a second PT, and a final ET to produce CO (referred to as the PCET pathway, or pathway B).[32,33] Finally, Xu et al. proposed a simplified version of the PCET pathway where the initial PCET is followed by a second PCET to form CO (pathway C).[25] In all three cases, if the initial step is rate limiting, regardless whether it is an ET or a PCET step, the expected Tafel slope is 118 mV dec^{-1}. If the PT following the initial ET (pathway A) or the initial PCET (pathway B) is rate limiting, both ET and PCET pathways are expected to show Tafel slopes of 59 mV dec^{-1}. A Tafel slope of 39 mV dec^{-1} is expected in each case if the second ET (pathway B) or PCET (pathway A) is rate limiting (assuming a symmetry factor, β, of 0.5), and a slope of 30 mV dec^{-1} is expected if CO desorption is the rate limiting step. It is possible that either the second electron transfer (steps A.3, B.3, or C.2) or CO desorption steps (steps A.4, B.3, or C.3) are rate-limiting and transport limitations caused by site blocking (by electrolyte cations) are inflating the observed Tafel slope. However, both alternatives are unlikely based on our spectroscopic observations. No band associated with the $COOH_{ad}$ intermediate, which would be expected to accumulate if the second electron transfer is rate-determining, is observed spectroscopically on polycrystalline Au electrodes.[25,41] CO desorption is unlikely to be rate limiting due to the low binding energy of CO on Au.[40] Moreover, cations have been shown to aid rather than inhibit CO desorption,[35] so that cation adsorption would not be expected to increase the observed Tafel slope in the case of CO desorption as the RLS. Therefore, based on the ∼59 mV dec^{-1} Tafel slope measured on both Au and Ag surfaces in the kinetic regime as discussed in the previous section, we conclude that regardless whether catalysts are polycrystalline or nanostructured in nature, the reaction is limited by a PT step preceded by an initial ET or PCET at low overpotentials.

Although Tafel analysis alone cannot distinguish exactly which pathway CO_2RR proceeds, several meaningful conclusions can still be drawn. First, a Tafel slope of ∼59 mV dec^{-1} is not expected for any step in pathway C, which indicates that it is unlikely for the CO_2RR on Au or Ag electrodes at low overpotentials. Meanwhile, ET and PCET pathways could both be consistent with the measured transport-limitation-free Tafel slope with the second PT step in each mechanism (steps A.2 and B.2) as the RLS. Although the stabilization of the $*CO_2^-$ intermediate via interaction with the electrode surface could make its formation potentially feasible when a suitable molecular catalyst is used, the formation of free $CO_2^{\bullet-}$ is energetically unfavorable (E^0 = −1.85 ± 0.06 V vs SHE).[42−44] One potential way to distinguish between the ET pathway and the PECT pathway is to study the rate dependency on the pH of the electrolyte. If step A.2 is the RLS, no pH dependence is expected (reaction order of $[H^+]$ is zero), as no PT occurs in step A.1. If step B.2 is the RLS, a first-order dependence on pH is expected (reaction order of $[H^+]$ is 1), owing to the PT in the equilibrated step B.1. As will be discussed in the next section, these seemingly straightforward studies can be complicated by the experimental difficulty in varying on parameter at a time due to multiple aqueous phase equilibria in the electrolyte.

INTERPLAY BETWEEN PROPOSED MECHANISM AND EXPERIMENTAL DESIGN

Standard Hydrogen Electrode versus Reversible Hydrogen Electrode Scale. In probing the rate dependence on pH, it is important to note that different mechanistic proposals could lead to different experimental designs and in turn seemingly inconsistent measured parameters (e.g., reaction orders of different species) even when experiments are conducted rigorously. Electrochemical potentials of all electrochemical transformations are defined on an absolute scale relative to that of the reaction of $H^+ + e^- \rightarrow 1/2H_2$ under standard conditions, or the SHE scale.[22] Meanwhile, for reactions that produce or consume protons (or hydroxides) in or preceding the RLS, the proton dependence can be accounted for either by correcting for this dependence when analyzing experimental results or by conducting experiments on a RHE scale. Experimentally, it is often more convenient to adopt the RHE scale, because the impact of the proton concentration (pH of the electrolyte) is explicitly taken into account such that the study of reaction order of other species is free from the convolution of proton dependence. Therefore, the assumed reaction mechanism and RLS dictate whether the SHE or the RHE scale is more suitable for a specific system. It must be emphasized that when all variables are properly accounted for, the two approaches, namely whether to conduct experiments on the SHE or the RHE scale, produce the same results. In the case of CO_2RR on Au, the ET pathway with either the first ET (step A.1) or first PT (step A.2) as the RLS, and the PCET pathway with first PT (step B.2) as the RLS suggest that the SHE and the RHE scale is more convenient, respectively. This discrepancy is due to the fact that the activity of proton (a_{H+}) does not appear in the rate expression of the former mechanism, but does in the latter (Table 1). Here, we show that this difference in assumed reaction mechanisms leads to different designs of experiments, which in turn causes conflicting reported values for the reaction order of bicarbonate.

The assumption of the ET pathway with either step A.1 or A.2 as the RLS in the CO_2RR on Au dictates that the CO production rate is pH independent. It follows naturally that all electrokinetic experiments, including those aiming at determining the reaction order of bicarbonate in the CO_2RR, should be, and indeed have been, conducted using the SHE scale.[28,29] CO production rate was found to have a zeroth-order dependence on bicarbonate concentration when bicarbonate concentration was varied, holding the cathode potential constant on the SHE scale.[28,29] This finding was interpreted as evidence confirming that the initial ET step (step A.1) was rate limiting.

In contrast, if step B.2 is the RLS as indicated by a Tafel slope of 59 mV dec^{-1} in the previous section, then the pH of the electrolyte must be accounted for since the RLS is

DOI: 10.1021/acscatal.8b02181
ACS Catal. 2018, 8, 8121−8129

proceeded by an equilibrated PCET step. It follows that rates should either be determined at a constant potential on the RHE scale, as it is the case in our previous study, or the dependence on a_{H+} should be accounted for when analyzing data collected at a constant SHE potential.[25] This consideration is particularly important in the determination of dependence of the CO production rate on bicarbonate concentration, as the pH of the CO_2-saturated solution increases with bicarbonate concentration. When the electrode potential for the CO_2RR was kept constant with respect to RHE, a roughly first-order dependence on bicarbonate was observed. Although a bicarbonate dependence is not explicitly predicted by the rate expressions unless bicarbonate, rather than water, is assumed to be the proton donor, the bicarbonate dependence arises through the enhancement of CO production rates via an increase in the effective $[CO_{2(aq)}]$ through the equilibrium between bicarbonate and $CO_{2(aq)}$ as detailed in our previous work.[25]

Despite seemingly contradicting results of bicarbonate dependence, the apparent discrepancies are largely caused by the assumed dependence on a_{H+}. For example, in the work by Surendranath et al., where bicarbonate exhibits a zeroth-order dependence, the pH of the electrolyte changes from 6.2 to 7.2 as the bicarbonate concentration is increased from 0.03 to 0.3 M.[29] In turn, a_{H+} decreases by an order of magnitude and the potential on the RHE scale (assuming step B.2 is rate limiting) decreases by 59 mV across the range of bicarbonate concentrations studied based on the Nernst equation (eq 4).[22]

$$\Delta E_{RHE} = \Delta E_{SHE} - \frac{2.3RT}{F}\log(a_{H^+}) \quad (4)$$

A dependence on bicarbonate concentration can be clearly observed (Figure 4) if each current density taken from Figure 3c of the work by Surendranath et al. is adjusted to account for a first-order dependence on a_{H+} using Tafel slopes of 59 or 118 mV dec^{-1}. If the Tafel slope is assumed to be 118 mV dec^{-1} at −0.9 V vs SHE, the rate exhibits a ∼0.5-order dependence on bicarbonate. If a Tafel slope of 59 mV dec^{-1} is assumed, the rate shows an approximate first-order dependence on bicarbonate concentration. This first-order dependence is consistent with our previous work conducted on the RHE scale.[25] This analysis demonstrates that the design of experiments, including on whether to control and account for changes in a_{H+} based on the proposed mechanism, can produce seemly contradictory results and consequentially different mechanistic conclusions even when experiments were done rigorously. This example underscores the importance of employing an independent method to verify mechanistic conclusions drawn solely from electrokinetic investigations.

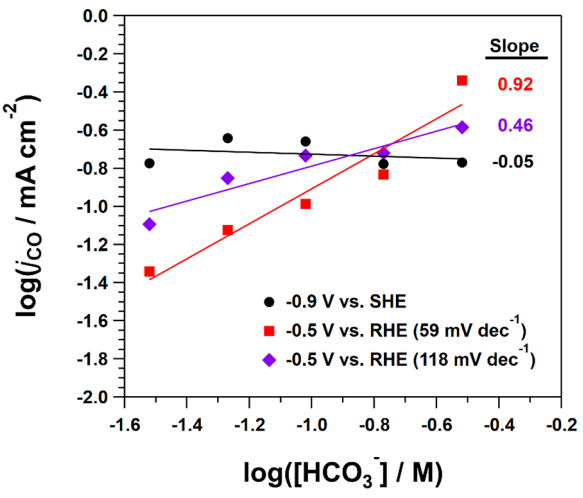

Figure 4. Bicarbonate order dependence data at −0.9 V vs SHE (black circles) and at −0.5 V vs RHE corrected for the pH changes with bicarbonate concentration assuming a Tafel slope of 59 mV dec^{-1} (red squares) and 118 mV dec^{-1} (purple diamonds). All data taken from ref 28.

Complications in Kinetic Isotope Effect Studies for CO_2RR. In addition to the concentration-dependence studies, kinetic isotope effect (KIE) studies could, in principle, provide useful information to elucidate if the RLS in CO_2RR involves a PT step. To effectively conduct and interpret KIE studies, one must study the relatively small changes in CO_2RR reaction rates when isotopically labeled proton donors, e.g., DCO_3^- or D_2O, are used in place of their nonlabeled counterparts while keeping all other variables constant (e.g., CO_2 solubility, temperature, solvation affects). However, in KIE studies of the CO_2RR, keeping all other variables constant while changing the proton donor is difficult. Changing the solvent (e.g., H_2O to D_2O) can lead to a variety of complicating factors such as differences in solvation of the electrolyte, changes in CO_2 solubility ($[CO_{2(aq)}]$ = 33.8 mM in H_2O, 38.1 mM in D_2O),[45] or differences in hydrogen bonding so that kinetic changes due solely to proton donation cannot be easily extracted. Kenis et al. conducted KIE studies in a flow cell, in which the catholyte is 2.0 M NaOD and the anolyte is 2.0 M NaOH to prevent changes in cell performance due to the KIE on the oxygen evolution reaction and the anode.[46] In addition to the possible change in mechanism due to reaction of CO_2 with NaOD to form $NaDCO_3$ at the cathode, the catholyte and anolyte are separated by an anion exchange membrane such that electrolyte crossover between the two compartments, especially at membrane on which catalysts are loaded, is likely if not inevitable. Any presence of NaOH and H_2O on the surface of cathodic catalyst could impact the measured KIE because H-containing species may preferentially react over D-containing species. In another work, batch experiments by Surendranath et al. were conducted in $NaHCO_3$ electrolytes with H/D ratios between 0.1 and 0.9.[28] Because relatively small changes in reaction rates are expected (typical KIE values are 1−2),[47] pure labeled and nonlabeled chemicals should be used as stated above. To further illustrate the complex nature of using KIE studies to elucidate the CO_2RR, the current density toward CO was measured on Au foil electrodes at a kinetically controlled potential (−0.4 V vs RHE) in both CO_2-saturated 0.5 M $NaHCO_3$ (in H_2O) and 0.5 M $NaDCO_3$ (in D_2O). Surprisingly, the current density toward CO is −0.070 ± 0.005 mA cm^{-2} in $NaHCO_3$ and −0.162 ± 0.011 mA cm^{-2} in $NaDCO_3$. Importantly, the rate of HER decreased in the deuterated electrolyte with current densities toward H_2 and D_2 of −0.077 ± 0.002 mA cm^{-2} and −0.039 ± 0.014 mA cm^{-2}, respectively. The inverse relationship between CO and H_2/D_2 rates suggests that the improved CO selectivity in the deuterated electrolyte may be due in large part to the decreased rate of the competing HER. The increased activity in deuterated electrolyte is likely a result of various convoluting factors mentioned above that cannot be easily decoupled, rather than indicating that the D-containing species accelerates the RLS compared to the H-containing counterpart (KIE < 1).

DOI: 10.1021/acscatal.8b02181
ACS Catal. 2018, 8, 8121−8129

Another recent example of unexpected KIE is that the rate of CO oxidation on Au/TiO_2 in aqueous solution is retarded by replacing H_2O with D_2O, while water is not expected to participate based on the overall reaction.[48] It is only through sophisticated first-principles computational studies is the role of water in the reaction mechanism elucidated. In light of the complexities in swapping all H-donors to D-donors, gaining mechanistic insights based on KIE experiments is nontrivial. Thus, accurate interpretation of the measured KIE regarding the role of proton donors in the CO_2RR in aqueous electrolytes is challenging.

OUTLOOK

Although electrokinetic studies can be informative in understanding reaction mechanisms of electrochemical processes, the relatively simple case of the two-electron CO_2RR to CO illustrates the inherent limitations of these techniques and underscores the necessity for the development of supporting spectroscopic and computational methods. Rigorous Tafel analysis can only be conducted in a full-kinetically controlled potential and current region to avoid transport limitations, which is often well outside of typical reaction conditions. As a result, reliable mechanistic insights can only be obtained at low overpotential and current densities, and possible changes in mechanistic pathway or RLS that occur at higher overpotentials and current densities cannot be directly investigated by Tafel analysis. Moreover, kinetic studies probing the dependence on different species can be heavily influenced by the proposed/assumed mechanism and experimental design. In the specific case of CO_2RR to CO on Au, it appears that the experimental design based on a specific proposed mechanism tends to reinforce the assumed mechanism. In order to effectively investigate CO_2RR to CO, along with more complicated electrochemical systems such as CO_2RR to C_{2+} products or N_2 reduction for ammonia production, it is necessary to leverage in situ/operando and time-resolved spectroscopic techniques such as ATR-SEIRAS and differential electrochemical mass spectroscopy to fill the gaps in mechanistic understanding left by traditional kinetics. Moreover, the continued development and improvement of computational methods for investigating the electrochemical processes, including the solvation and other electrolyte effects, is necessary for elucidating electrochemical reaction mechanisms. In the relatively simple two-electron process of CO_2RR to CO on Au and Ag, combined spectroscopic and electrokinetic studies have narrowed reaction pathways down to either an initial ET to $*CO_2^-$ or a PCET to *COOH. First-principles calculations of the stability of the possible intermediates (e.g., $*CO_2^-$), and the activation barriers for proposed RLS could help differentiate these two potential mechanisms. Without a doubt, intimate interplay between experimental and computational investigations will be indispensable in gaining molecular level understanding of more complex heterogeneous electrocatalytic reactions.

EXPERIMENTAL SECTION

Materials. To prepare Ag electrode for electrochemical kinetic experiments, bulk Ag foil was purchased from Alfa Aesar (99.998%). Five 15 mm × 7 mm Ag foil pieces were cut and then spot-welded together at one end to construct a fan-type structure in order to increase the total exposed surface area. Finally, a Ag wire was connected to one end of the electrode via spot-welding. The as-prepared electrode was etched in piranha solution (3:1 volumetric ratio of 98% H_2SO_4 (Sigma-Aldrich) and 30% H_2O_2 (Sigma-Aldrich)) for 20 s and then rinsed/sonicated using doubled deionized-stilled water (Barnstead Mega-Pure Water Purification System) for subsequent electrochemical studies. Purified 0.5 M $NaHCO_3$ electrolyte was prepared by purging a solution made from Na_2CO_3 (Fluka, ≥ 99.999%) with CO_2 gas (Keengas, grade 5) until the solution reached a pH value of 7.2. The electrolyte was then purified using a solid-supported iminodiacetate resin (Chelex 100, Sigma-Aldrich).[49]

To prepare electrodes for kinetic isotope experiments, bulk Au foil was purchased from Alfa Aesar (99.999%) and cut into planar electrode with dimensions of 14 mm × 6 mm. Finally, an Au wire connected to one end of the planar electrode via spot-welding. The electrode was then etched in cleaned in piranha etch for >5 min and rinsed using double deionized−distilled water (Barnstead Mega-Pure Water Purification System) prior to each electrolysis. $NaHCO_3$ electrolyte was prepared as detailed for electrolysis experiments using Ag electrodes. $NaDCO_3$ electrolyte was prepared by purging a solution made from Na_2CO_3 (Fluka, > 99.9999%) in D_2O (Arcos Organics, > 99.8%) overnight with high purity CO_2 gas (Keengas, grade 5). The electrolyte was then purified using a solid-supported iminodiacetate resin (Chelex 100, Sigma-Aldrich) which had been exchanged by soaking in D_2O for >24 h prior to use. The anion exchange membrane (Fumasep, FAA-3-PK-130) was also soaked for >24 h in D_2O before electrolysis to prevent additional H_2O from entering the deuterated electrolyte.

Electrochemical Kinetics Experiments. A Princeton Applied Research VersaSTAT 3 potentiostat was used for electrolysis experiments. Electrolysis experiments were conducted under room temperature in a gastight two compartment electrochemical cell using an anion exchange membrane (Fumasep, FAA-3-PK-130) as the separator. The working electrode compartment contained 13 mL of electrolyte and 9 mL of headspace. A high purity graphite rod was used as the counter electrode in all experiments to avoid any potential contamination issues. All potentials were measured against a Ag/AgCl reference electrode (3.0 M KCl, BASi) and converted to the RHE reference scale. Before electrolysis, the electrolyte and headspace were purged with CO_2 gas and then sealed. During electrolysis, the electrolyte in both compartments was stirred at a rate of 800 rpm using a magnetic stirrer. A gas chromatograph (Agilent, 7890B) was used for quantification. Constant potential experiments were conducted for 1 h or 30 min on Ag and Au electrodes, respectively. Gas-phase products were collected and injected into the gas chromatograph using a gastight syringe (Hamilton) for quantification of CO and H_2.

ATR-SEIRAS Experiments. ATR-SEIRAS experiments were conducted in a two-compartment spectroelectrochemical cell as described in our previous work.[25] The working electrode was an Au film chemically deposited on a Si ATR crystal with a 60 degree incident angle. A detailed procedure for preparation of the Au film electrode is given in our previous work. A graphite rod, rather than a Pt wire was used as the counter electrode to prevent contamination of the Au working electrode by Pt deposition from the counter electrode. A Ag/AgCl (3.0 M KCl, BASi) reference electrode was used in the working electrode compartment for all experiments. The working and counter electrode compartments were separated using a Nafion proton exchange membrane. Spectra were

DOI: 10.1021/acscatal.8b02181
ACS Catal. 2018, 8, 8121−8129

collected during cyclic voltammetry in 0.1 M $KClO_4$ (>99.99% metals basis, Sigma-Aldrich), under continuous CO purge (Matheson). All spectroscopic data was collected using an Agilent Technologies Cary 660 FTIR spectrometer equipped with a liquid nitrogen-cooled MCT detector and a Pike Technologies VeeMAX II ATR accessory coupled with a Solartron SI 1260/1287 system for electrochemical measurements.

AUTHOR INFORMATION

Corresponding Authors

*E-mail: yanys@udel.edu.
*E-mail: jiao@udel.edu
*E-mail: bxu@udel.edu

ORCID

Yushan Yan: 0000-0001-6616-4575
Feng Jiao: 0000-0002-3335-3203
Bingjun Xu: 0000-0002-2303-257X

Author Contributions

†(M.D., W.L.) These authors contributed equally to this work.

Notes

The authors declare no competing financial interest.

ACKNOWLEDGMENTS

W.L. and F.J. would like to acknowledge the National Science Foundation CAREER Program (Award No. CBET-1350911) for financial support. M.D. and Y.Y. would like to acknowledge the National Science Foundation−Chemical Catalysis Program (Award No. CHE- 1566138). B.X. would like to acknowledge the National Science Foundation CAREER Program (Award No. CBET-1744586) for financial support.

REFERENCES

(1) Jiao, Y.; Zheng, Y.; Jaroniec, M.; Qiao, S. Z. Design of Electrocatalysts for Oxygen-and Hydrogen-Involving Energy Conversion Reactions. *Chem. Soc. Rev.* **2015**, *44* (8), 2060−2086.

(2) Whipple, D. T.; Kenis, P. J. A. Prospects of CO_2 Utilization via Direct Heterogeneous Electrochemical Reduction. *J. Phys. Chem. Lett.* **2010**, *1* (24), 3451−3458.

(3) van der Ham, C. J. M.; Koper, M. T. M.; Hetterscheid, D. G. H. Challenges in Reduction of Dinitrogen by Proton and Electron Transfer. *Chem. Soc. Rev.* **2014**, *43* (15), 5183−5191.

(4) Seh, Z. W.; Kibsgaard, J.; Dickens, C. F.; Chorkendorff, I.; Nørskov, J. K.; Jaramillo, T. F. Combining Theory and Experiment in Electrocatalysis: Insights into Materials Design. *Science* **2017**, *355* (6321), eaad4998.

(5) Hori, Y.; Takahashi, R.; Yoshinami, Y.; Murata, A. Electrochemical Reduction of CO at a Copper Electrode. *J. Phys. Chem. B* **1997**, *101* (36), 7075−7081.

(6) Bertheussen, E.; Verdaguer-Casadevall, A.; Ravasio, D.; Montoya, J. H.; Trimarco, D. B.; Roy, C.; Meier, S.; Wendland, J.; Nørskov, J. K.; Stephens, I. E. L.; Chorkendorff, I. Acetaldehyde as an Intermediate in the Electroreduction of Carbon Monoxide to Ethanol on Oxide-Derived Copper. *Angew. Chem., Int. Ed.* **2016**, *55* (4), 1450−1454.

(7) Birdja, Y. Y.; Koper, M. T. M. The Importance of Cannizzaro-Type Reactions during Electrocatalytic Reduction of Carbon Dioxide. *J. Am. Chem. Soc.* **2017**, *139* (5), 2030−2034.

(8) Yeo, B. S.; Klaus, S. L.; Ross, P. N.; Mathies, R. A.; Bell, A. T. Identification of Hydroperoxy Species as Reaction Intermediates in the Electrochemical Evolution of Oxygen on Gold. *ChemPhysChem* **2010**, *11* (9), 1854−1857.

(9) Trześniewski, B. J.; Diaz-Morales, O.; Vermaas, D. A.; Longo, A.; Bras, W.; Koper, M. T. M.; Smith, W. A. Situ Observation of Active Oxygen Species in Fe-Containing Ni-Based Oxygen Evolution Catalysts: The Effect of pH on Electrochemical Activity. *J. Am. Chem. Soc.* **2015**, *137* (48), 15112−15121.

(10) Shinagawa, T.; Garcia-Esparza, A. T.; Takanabe, K. Insight on Tafel slopes from a microkinetic analysis of aqueous electrocatalysis for energy conversion. *Sci. Rep.* **2015**, *5*, 13801.

(11) Bockris, J. O. M.; Ammar, I. A.; Huq, A. K. M. S. The Mechanism of the Hydrogen Evolution Reaction on Platinum, Silver and Tungsten surfaces in Acid Solutions. *J. Phys. Chem.* **1957**, *61* (7), 879−886.

(12) Kunimatsu, K.; Senzaki, T.; Samjeské, G.; Tsushima, M.; Osawa, M. Hydrogen Adsorption and Hydrogen Evolution Reaction on a Polycrystalline Pt Electrode Studied by Surface-Enhanced Infrared Absorption Spectroscopy. Electrochim. *Electrochim. Acta* **2007**, *52* (18), 5715−5724.

(13) Marković, N. M.; Grgur, B. N.; Ross, P. N. Temperature-Dependent Hydrogen Electrochemistry on Platinum Low-Index Single-Crystal Surfaces in Acid Solutions. *J. Phys. Chem. B* **1997**, *101* (27), 5405−5413.

(14) Zheng, J.; Yan, Y.; Xu, B. Correcting the Hydrogen Diffusion Limitation in Rotating Disk Electrode Measurements of Hydrogen Evolution Reaction Kinetics. *J. Electrochem. Soc.* **2015**, *162* (14), F1470−F1481.

(15) Antoine, O.; Bultel, Y.; Durand, R. Oxygen Reduction Reaction Kinetics and Mechanism on Platinum Nanoparticles Inside Nafion®. *J. Electroanal. Chem.* **2001**, *499* (1), 85−94.

(16) Parthasarathy, A.; Martin, C. R.; Srinivasan, S. Investigations of the O_2 Reduction Reaction at the Platinum/Nafion® Interface Using a Solid-State Electrochemical Cell. *J. Electrochem. Soc.* **1991**, *138* (4), 916−921.

(17) Wang, J. X.; Uribe, F. A.; Springer, T. E.; Zhang, J.; Adzic, R. R. Intrinsic Kinetic Equation for Oxygen Reduction Reaction in Acidic Media: the Double Tafel Slope and Fuel Cell Applications. *Faraday Discuss.* **2009**, *140* (0), 347−362.

(18) Holewinski, A.; Linic, S. Elementary Mechanisms in Electrocatalysis: Revisiting the ORR Tafel Slope. *J. Electrochem. Soc.* **2012**, *159* (11), H864−H870.

(19) Da Silva, L. M.; Boodts, J. F. C.; De Faria, L. A. Oxygen Evolution at $RuO_{2(x)}$+$Co_3O_{4(1-x)}$ Electrodes from Acid Solution. Electrochim. *Electrochim. Acta* **2001**, *46* (9), 1369−1375.

(20) Hu, J.-M.; Zhang, J.-Q.; Cao, C.-N. Oxygen Evolution Reaction on IrO_2-Based DSA® Type Electrodes: Kinetics Analysis of Tafel Lines and EIS. *Int. J. Hydrogen Energy* **2004**, *29* (8), 791−797.

(21) Liang, Z. X.; Zhao, T. S.; Xu, J. B.; Zhu, L. D. Mechanism Study of the Ethanol Oxidation Reaction on Palladium in Alkaline Media. Electrochim. *Electrochim. Acta* **2009**, *54* (8), 2203−2208.

(22) Bard, A. J.; Faulkner, L. R. *Electrochemical Methods: Fundamentals and Applications*, 2nd ed., Wiley: New York, 2000.

(23) Durst, J.; Siebel, A.; Simon, C.; Hasché, F.; Herranz, J.; Gasteiger, H. A. New Insights into the Electrochemical Hydrogen Oxidation and Evolution Reaction Mechanism. *Energy Environ. Sci.* **2014**, *7*, 2255−2260.

(24) Chen, Y.; Li, C. W.; Kanan, M. W. Aqueous CO_2 Reduction at Very Low Overpotential on Oxide-Derived Au Nanoparticles. *J. Am. Chem. Soc.* **2012**, *134* (49), 19969−19972.

(25) Dunwell, M.; Lu, Q.; Heyes, J. M.; Rosen, J.; Chen, J. G.; Yan, Y.; Jiao, F.; Xu, B. The Central Role of Bicarbonate in the Electrochemical Reduction of Carbon Dioxide on Gold. *J. Am. Chem. Soc.* **2017**, *139* (10), 3774−3783.

(26) Hori, Y.; Murata, A.; Kikuchi, K.; Suzuki, S. Electrochemical Reduction of Carbon Dioxides to Carbon Monoxide at a Gold Electrode in Aqueous Potassium Hydrogen Carbonate. *J. Chem. Soc., Chem. Commun.* **1987**, *10*, 728−729.

(27) Noda, H.; Ikeda, S.; Yamamoto, A.; Einaga, H.; Ito, K. Kinetics of Electrochemical Reduction of Carbon Dioxide on a Gold Electrode in Phosphate Buffer Solutions. *Bull. Chem. Soc. Jpn.* **1995**, *68* (7), 1889−1895.

(28) Wuttig, A.; Yaguchi, M.; Motobayashi, K.; Osawa, M.; Surendranath, Y. Inhibited Proton Transfer Enhances Au-catalyzed

DOI: 10.1021/acscatal.8b02181
ACS Catal. 2018, 8, 8121−8129

CO_2-to-Fuels Selectivity. *Proc. Natl. Acad. Sci. U. S. A.* **2016**, *113* (32), E4585−E4593.
(29) Wuttig, A.; Yoon, Y.; Ryu, J.; Surendranath, Y. Bicarbonate Is Not a General Acid in Au-Catalyzed CO_2 Electroreduction. *J. Am. Chem. Soc.* **2017**, *139* (47), 17109−17113.
(30) Zhu, W.; Michalsky, R.; Metin, Ö.; Lv, H.; Guo, S.; Wright, C. J.; Sun, X.; Peterson, A. A.; Sun, S. Monodisperse Au Nanoparticles for Selective Electrocatalytic Reduction of CO_2 to CO. *J. Am. Chem. Soc.* **2013**, *135* (45), 16833−16836.
(31) Hori, Y. Electrochemical CO2 Reduction on Metal Electrodes. In *Modern Aspects of Electrochemistry*; Vayenas, C., White, R., Gamboa-Aldeco, M., Eds.; Springer: New York, 2008; Vol. *42*, pp 89−189.
(32) Hatsukade, T.; Kuhl, K. P.; Cave, E. R.; Abram, D. N.; Jaramillo, T. F. Insights into the Electrocatalytic Reduction of CO_2 on Metallic Silver Surfaces. *Phys. Chem. Chem. Phys.* **2014**, *16* (27), 13814−13819.
(33) Rosen, J.; Hutchings, G. S.; Lu, Q.; Rivera, S.; Zhou, Y.; Vlachos, D. G.; Jiao, F. Mechanistic Insights into the Electrochemical Reduction of CO_2 to CO on Nanostructured Ag Surfaces. *ACS Catal.* **2015**, *5* (7), 4293−4299.
(34) Mills, J. N.; McCrum, I. T.; Janik, M. J. Alkali Cation Specific Adsorption onto fcc(111) Transition Metal Electrodes. *Phys. Chem. Chem. Phys.* **2014**, *16* (27), 13699−13707.
(35) Dunwell, M.; Wang, J.; Yan, Y.; Xu, B. Surface Enhanced Spectroscopic Investigations of Adsorption of Cations on Electrochemical Interfaces. *Phys. Chem. Chem. Phys.* **2017**, *19* (2), 971−975.
(36) Blizanac, B. B.; Arenz, M.; Ross, P. N.; Marković, N. M. Surface Electrochemistry of CO on Reconstructed Gold Single Crystal Surfaces Studied by Infrared Reflection Absorption Spectroscopy and Rotating Disk Electrode. *J. Am. Chem. Soc.* **2004**, *126* (32), 10130−10141.
(37) Kunimatsu, K.; Aramata, A.; Nakajima, N.; Kita, H. Infrared Spectra of Carbon Monoxide Adsorbed on a Smooth Gold Electrode. *J. Electroanal. Chem. Interfacial Electrochem.* **1986**, *207* (1), 293−307.
(38) Miyake, H.; Ye, S.; Osawa, M. Electroless Deposition of Gold Thin Films on Silicon for Surface-Enhanced Infrared Spectroelectrochemistry. *Electrochem. Commun.* **2002**, *4* (12), 973−977.
(39) Pronkin, S.; Hara, M.; Wandlowski, T. Electrocatalytic Properties of Au(111)-Pd Quasi-Single-Crystal Film Electrodes as Probed by ATR-SEIRAS. *Russ. J. Electrochem.* **2006**, *42* (11), 1177−1192.
(40) Shi, C.; Hansen, H. A.; Lausche, A. C.; Norskov, J. K. Trends in Electrochemical CO_2 Reduction Activity for Open and Close-Packed Metal Surfaces. *Phys. Chem. Chem. Phys.* **2014**, *16* (10), 4720−4727.
(41) Dunwell, M.; Yan, Y.; Xu, B. Situ Infrared Spectroscopic Investigations of Pyridine-Mediated CO_2 Reduction on Pt Electrocatalysts. *ACS Catal.* **2017**, *7* (8), 5410−5419.
(42) Schwarz, H.; Dodson, R. Reduction Potentials of CO_2-and the Alcohol Aadicals. *J. Phys. Chem.* **1989**, *93* (1), 409−414.
(43) Surdhar, P. S.; Mezyk, S. P.; Armstrong, D. A. Reduction Potential of the Carboxyl Radical Anion in Aqueous Solutions. *J. Phys. Chem.* **1989**, *93* (8), 3360−3363.
(44) Sakaki, S. An Ab Initio MO/SD-CI Study of Model Complexes of Intermediates in Electrochemical Reduction of Carbon Dioxide Catalyzed by $NiCl_2$(cyclam). *J. Am. Chem. Soc.* **1992**, *114* (6), 2055−2062.
(45) Pocker, Y.; Bjorkquist, D. W. Stopped-flow Studies of Carbon Dioxide Hydration and Bicarbonate Dehydration in Water and Water-d2. Acid-base and Metal Ion Catalysis. *J. Am. Chem. Soc.* **1977**, *99* (20), 6537−6543.
(46) Verma, S.; Hamasaki, Y.; Kim, C.; Huang, W.; Lu, S.; Jhong, H.-R. M.; Gewirth, A. A.; Fujigaya, T.; Nakashima, N.; Kenis, P. J. A. Insights into the Low Overpotential Electroreduction of CO_2 to CO on a Supported Gold Catalyst in an Alkaline Flow Electrolyzer. *ACS Energy Lett.* **2018**, *3* (1), 193−198.
(47) Anslyn, E. V.; Dougherty, D. A. *Modern Physical Organic Chemistry*; University Science Books: Herndon, VA, 2006.
(48) Saavedra, J.; Doan, H. A.; Pursell, C. J.; Grabow, L. C.; Chandler, B. D. The Critical Role of Water at the Gold-Titania Interface in Catalytic CO Oxidation. *Science* **2014**, *345* (6204), 1599.
(49) Wuttig, A.; Surendranath, Y. Impurity Ion Complexation Enhances Carbon Dioxide Reduction Catalysis. *ACS Catal.* **2015**, *5* (7), 4479−4484.

DOI: 10.1021/acscatal.8b02181
ACS Catal. 2018, 8, 8121−8129